

An Adjoint-Free Algorithm for CNOP via Sampling

Bin Shi* ^{1,3} and Guodong Sun^{2,3}

¹*State Key Laboratory of Scientific and Engineering Computing, Academy of Mathematics and Systems Science, Chinese Academy of Sciences, Beijing 100190, China*

²*State Key Laboratory of Numerical Modeling for Atmospheric Sciences and Geophysical Fluid Dynamics, Institute of Atmospheric Physics, Chinese Academy of Sciences, Beijing 100029, China*

³*University of Chinese Academy of Sciences, Beijing 100049, China*

August 18, 2022

Abstract

In this paper, we propose a sampling algorithm based on statistical machine learning to obtain conditional nonlinear optimal perturbation (CNOP), which is essentially different from the traditional deterministic optimization methods. The new approach not only reduces the extremely expensive gradient (first-order) information directly by the objective value (zeroth-order) information but also avoids the use of the adjoint technique that gives rise to the enormous storage problem and the instability from linearization. Meanwhile, an intuitive analysis of the sampling algorithm is shown rigorously within a form of a concentration inequality for the approximate gradient. The numerical experiments of a theoretical model, Burgers equation with small viscosity, to obtain the CNOPs by the performance of standard spatial structures demonstrate that at the cost of losing accuracy, fewer samples spend time relatively shorter than the adjoint-based method and directly from the definition. Finally, we reveal that the nonlinear time evolution of the CNOPs obtained by all the algorithms is almost consistent with the quantity of norm square of perturbations, their difference, and relative difference based on the definition method.

1 Introduction

The short-term behavior of a predictive model with imperfect initial data is one of the critical issues for weather and climate predictability. Understanding the model's sensitivity to errors in the initial data to assessing subsequent errors in forecasts is indispensable. Perhaps, the simplest and most practical way is to estimate the likely uncertainty in the forecast by considering an ensemble of runs with initial data polluted by the most dangerous errors. Traditionally from the linear stability analysis of fluid dynamics, the well-known tool is normal mode [Rayleigh, 1879, Lin, 1955], which has been adopted to understand and analyze the observed cyclonic waves and long waves of middle and high latitudes [Eady, 1949]. However, the atmospheric and oceanic modes are often unstable; that is, the transient growth of perturbations can still occur in the absence of growing normal modes [Farrell and Ioannou, 1996a,b]. Therefore, the normal mode theory is

*Corresponding author: shibin@lsec.cc.ac.cn

generally unavailable for the predictability problem generated by atmospheric and oceanic motion flows. To serve this purpose for a low-order two-layer quasi-geostrophic model in a periodic channel, [Lorenz \[1965\]](#) first proposes a nonnormal mode approach based on the view of linearization, which introduces the concepts of the tangent linear model, adjoint model, singular values, and singular vectors. Then, [Farrell \[1982\]](#) utilizes the linear approach to investigate the linear instability within finite time. In the last decade of the past century, such a linear approach has been widely used to find the most dangerous perturbations of atmospheric and oceanic flows and has been extended to explore error growth and predictability, such as patterns of the general atmospheric circulations [[Buizza and Palmer, 1995](#)], the coupled ocean-atmosphere model of El Niño-Southern Oscillation (ENSO) [[Xue et al., 1997a,b](#), [Thompson, 1998](#), [Samelson and Tziperman, 2001](#)]. The nonnormal approach has recently been extended to an oceanic study, which is employed to investigate the predictability of the Atlantic meridional overturning circulation [[Zanna et al., 2011](#)] and the Kuroshio path variations [[Fujii et al., 2008](#)], respectively.

Both the approaches of normal and nonnormal modes are based on the assumption of linearization; that is, the perturbation is required so sufficiently small that a tangent linear model can approximately represent the evolution of the perturbation. The complex nonlinear atmospheric and oceanic processes have not still been well considered. To overcome this limitation, [Mu \[2000\]](#) proposes a nonlinear nonnormal mode approach, which introduces the concepts of nonlinear singular value and nonlinear singular vector and then is employed to successfully capture the local fastest-growing perturbations for a 2D quasi-geostrophic model [[Mu and Wang, 2001](#)]. However, several disadvantages still exist, such as practical inconvenience, unreasonable physics of the large norm for local fastest growing perturbations, etc. Starting from the view of nonlinear programming, [Mu et al. \[2003\]](#) proposes an innovative approach, named conditional nonlinear optimal perturbation (CNOP), to explore the optimal perturbation that can fully consider the nonlinear effect without any linear approximation assumption. Generally speaking, the CNOP approach captures the initial perturbations with maximal nonlinear evolution given by a reasonable constraint in physics. Therefore, the CNOP approach as a powerful tool has been employed widely to investigate the fastest-growing initial error in the prediction of an atmospheric and oceanic event and reveal the related mechanism, such as the stability of the thermohaline circulation [[Mu et al., 2004](#), [Zu et al., 2016](#)], the predictability of ENSO [[Duan et al., 2009](#), [Duan and Hu, 2016](#)] and the Kuroshio path variations [[Wang and Mu, 2015](#)], the parameter sensitivity of the land surface processes [[Sun and Mu, 2017](#)], typhoon-targeted observations [[Mu et al., 2009](#), [Qin and Mu, 2012](#)]. For more details, please refer to the review paper [[Wang et al., 2020](#)] and more perspectives on the fields of fluid mechanics [[Kerswell, 2018](#)].

The pivotal for obtaining CNOPs is implementing nonlinear programming efficiently and effectively. Generally speaking, the nonlinear optimization methods adopted in practice are the spectral projected gradient method [[Birgin et al., 2000](#)], sequential quadratic programming [[Barclay et al., 1998](#)] and the limited memory Broyden-Fletcher-Goldfarb-Shanno algorithm [[Liu and Nocedal, 1989](#)]. In the field of fluid mechanics, the standard gradient method is adopted to obtain the minimal finite amplitude disturbance that triggers the transition to turbulence in shear flows [[Pringle and Kerswell, 2010](#)], and the method of Lagrange multipliers to investigate perturbations that maximize the gain of disturbance energy in 2D isolated vortex and counter-rotating vortex-pair [[Navrose et al., 2018](#)]. Here, the objective function in a black-box model for the initial perturbations is obtained by the time evolution of a nonlinear differential equation. Hence, the essential difficulty here in computation is how to get the gradient information efficiently. It is not practical to obtain gradient directly

from the definition-based methods, which need plenty of runs of the nonlinear model. Traditionally, the gradient information adopted in practice named the adjoint-based method is to calculate the tangent linear model and the adjoint matrix [Kalnay, 2003]. However, the adjoint-based method can only deal with smooth programming and is quite unstable for the atmospheric and oceanic models in practice. Furthermore, a massive storage space to save the basic state during each iteration is also a significant shortcoming, which causes the challenges of drastically high-dimensional optimization problems, data storage, and timeliness. Moreover, the current adjoint-free computational approaches still have their faults. Take the two cases as examples; the ensemble-based methods still require colossal memory and repeated calculations [Wang and Tan, 2010, Chen et al., 2015], and the intelligent optimization methods without any guarantee to find an optimal solution [Zheng et al., 2017, Yuan et al., 2015].

To overcome the weaknesses of the adjoint-based method above, we start from the view of stochastic optimization methods, which have been the workhorse algorithms powering recent developments in statistical machine learning [Bottou et al., 2018]. In this paper, we adopt the derivative-free method proposed by Nemirovski and Yudin [1983, Section 9.3.2], which is based on the simple high-dimensional divergence theorem (or Stokes’ theorem). Following the popular and natural way, the derivative-free method is a stochastic approximation-type method, which imitates a stochastic oracle of the first order by the available stochastic order of the zeroth order. And then, based on the law of large numbers, we utilize it by sampling and propose the concentration estimate by the general Hoeffding’s inequality. The basic description of the CNOP settings and the proposed sample-based algorithm are given in Section 2 and Section 3, respectively. We take a preliminary numerical test for the simple Burgers equation with small viscosity in Section 4. Summary and discussion are included in Section 5.

2 The Basic CNOP Settings

In this section, we give a brief description of the CNOP approach. Currently, the CNOP approach has been extended to investigate the influences of parameter and boundary condition errors on an atmospheric and oceanic model by exploring the impact of initial errors [Mu and Wang, 2017]. Here, we only focus on the initial perturbations. The atmospheric and oceanic model in a region $x \in \Omega \subseteq \mathbb{R}^d$ with $\partial\Omega$ as its boundary is given as

$$\begin{cases} \frac{\partial U}{\partial t} = F(U, P) \\ U|_{t=0} = U_0 \\ U|_{\partial\Omega} = G, \end{cases} \quad (2.1)$$

where U is the reference state in the configuration space, P is the model parameters, F is a nonlinear operator, and U_0 and G are the initial reference state and boundary condition, respectively. Without loss of generality, we note $g^t(\cdot)$ as the reference state $U(t; \cdot)$ in the configuration space evolving with time. Hence, given the initial condition U_0 , we can obtain the reference state at time T is $g^T(U_0) = U(T; U_0)$. If we consider the initial state $U_0 + u_0$ as the perturbation of U_0 , then the reference state at time T is given by $g^T(U_0 + u_0) = U(T; U_0 + u_0)$.

With both the reference states $g^T(U_0)$ and $g^T(U_0 + u_0)$, the objective function about the perturbation u_0 based on the initial condition U_0 for optimization can be proposed as

$$J(u_0; U_0) = \|g^T(U_0 + u_0) - g^T(U_0)\|^2, \quad (2.2)$$

and then the CNOP formulated as the constrained optimization problem is

$$\max_{\|u_0\| \leq \delta} J(u_0; U_0). \quad (2.3)$$

Both the objective function (2.2) and the optimization problem (2.3) come directly from the model (2.1), which is a theoretical model, hence infinite-dimensional. Furthermore, when numerical computation is utilized, the optimization problem of infinite dimension is reduced to finite dimension. Without loss of generality, we shorten $J(u_0; U_0)$ as $J(u_0)$ afterward for convenience.

3 The sample-based algorithm

In this section, we briefly describe the sample-based algorithm and conclude with a formal theorem for the concentration estimate of the approximate gradient. However, the detailed proof is deferred to Appendix A. The sample-based algorithm is composed of two steps. Firstly for the population case, we transform the expectation of gradient on the unit ball to that of objective values on the unit sphere by the high-dimensional Stokes' theorem. Then, we demonstrate an intuitive analysis of the concentration in probability for the samples with the law of large numbers.

Let \mathbb{B}^d be the unit ball in \mathbb{R}^d and $v_0 \sim \text{Unif}(\mathbb{B}^d)$, a random variable following the uniform distribution in \mathbb{B}^d . Given a small real $\epsilon > 0$, then we can define the expectation of J in the unit ball centering on u_0 as

$$\hat{J}(u_0) = \mathbb{E}_{v_0 \in \mathbb{B}^d} [J(u_0 + \epsilon v_0)]. \quad (3.1)$$

Obviously, the objective function J is needed to define in the ball $B(0; \delta + \epsilon) = \{u_0 \in \mathbb{R}^d : \|u_0\| \leq \epsilon + \delta\}$ ¹. Furthermore, we can find $\hat{J}(u_0)$ is approximate to $J(u_0)$, that is, $\hat{J}(u_0) \approx J(u_0)$. If the gradient ∇J exists in the ball $B(0; \delta + \epsilon)$, the fact that the expectation of v_0 is zero tells us the error estimate for the objective value is

$$\|J(u_0) - \hat{J}(u_0)\| = O(\epsilon^2).$$

With the representation of $\hat{J}(u_0)$ in (3.1), we can obtain the gradient $\nabla \hat{J}(u_0)$ directly from the function value J by the high-dimensional Stokes' theorem, that is,

$$\nabla \hat{J}(u_0) = \mathbb{E}_{v_0 \in \mathbb{B}^d} [\nabla J(u_0 + \epsilon v_0)] = \frac{d}{\epsilon} \cdot \mathbb{E}_{v_0 \in \mathbb{S}^{d-1}} [J(u_0 + \epsilon v_0) v_0], \quad (3.2)$$

where the random variable v_0 follows the uniform distribution on the unit sphere $\mathbb{S}^{d-1} = \partial \mathbb{B}^d$ in the last equality. Similarly, $\nabla \hat{J}(u_0)$ is approximate to $\nabla J(u_0)$, that is, $\nabla \hat{J}(u_0) \approx \nabla J(u_0)$. If the gradient ∇J exists in the ball $B(0; \delta + \epsilon)$, we can show the error estimate of the gradient is

$$\|\nabla \hat{J}(u_0) - \nabla J(u_0)\| = O(d\epsilon). \quad (3.3)$$

The rigorous description and proof are shown in Lemma A.1 with its proof of Appendix A.

¹Throughout the paper, the norm $\|\cdot\|$ is defined as the Euclidean norm, that is,

$$\|v\| = \sqrt{\sum_{i=1}^d v_i^2}.$$

Next, we demonstrate a simple but intuitive analysis of the convergence in probability for the samples in practice. With the representation of $\nabla \hat{J}(u_0)$ in (3.2), the weak law of large numbers states that the sample average converges in probability towards the expected value. That is, for any $t > 0$, we have

$$\Pr \left(\left\| \frac{d}{n\epsilon} \sum_{i=1}^n J(u_0 + \epsilon v_{0,i}) v_{0,i} - \nabla \hat{J}(u_0) \right\| \geq t \right) \rightarrow 0, \quad \text{with } n \rightarrow \infty.$$

Combined with the error estimate of gradient (3.3), if t is assumed to be larger than $\Omega(d\epsilon)$, that is, there exists a constant $\tau > 0$ such that $t > \tau d\epsilon$, the probability that the sample average approximates to $\nabla J(u_0)$ satisfies

$$\Pr \left(\left\| \frac{d}{n\epsilon} \sum_{i=1}^n J(u_0 + \epsilon v_{0,i}) v_{0,i} - \nabla J(u_0) \right\| \geq t - O(d\epsilon) \right) \rightarrow 0, \quad \text{with } n \rightarrow \infty.$$

Finally, we conclude the section with the rigorous Chernoff-type bound in probability for the simple but intuitive analysis above as the following theorem. The rigorous proof is shown in Appendix A with Lemma A.2 and Lemma A.3 proposed.

Theorem 1. If J is continuously differentiable and satisfies the gradient Lipschitz condition, that is, there exists a constant $L > 0$ such that for any $u_{0,1}, u_{0,2} \in B(0, \delta)$, we have

$$\|\nabla J(u_{0,1}) - \nabla J(u_{0,2})\| \leq L \|u_{0,1} - u_{0,2}\|.$$

For any $t > Ld\epsilon/2$, there exists a constant $C > 0$ such that the concentration inequality for samples is satisfied, that is,

$$\Pr \left(\left\| \frac{d}{n\epsilon} \sum_{i=1}^n J(u_0 + \epsilon v_{0,i}) v_{0,i} - \nabla J(u_0) \right\| \geq t - \frac{Ld\epsilon}{2} \right) \leq 2 \exp(-Cnt^2).$$

4 Model and numerical experiments

In this section, we take several numerical experiments to compare the proposed sample-based algorithms with the baseline algorithms for a theoretical model, Burgers equation with small viscosity. After the concept of CNOP is put forward [Mu et al., 2003], there have been several methods, adjoint-based or adjoint-free, proposed to obtain the CNOPs [Wang and Tan, 2010, Chen et al., 2015, Zheng et al., 2017, Yuan et al., 2015]. However, the essential difficulties, such as a massive storage space to save the basic state and instability when running an atmospheric and oceanic model, have still not been overcome. Here, different from the traditional deterministic optimization methods above, we obtain the approximate gradient by sampling objective values introduced in Section 3. Then we employ the second spectral projected gradient method (SPG2) proposed in [Birgin et al., 2000] to obtain the CNOPs.

We consider the simple theoretical model, Burgers equation with small viscosity under the Dirichlet condition that describes the nonlinear time evolution of the reference state u as

$$\begin{cases} \frac{\partial U}{\partial t} + U \frac{\partial U}{\partial x} = \gamma \frac{\partial^2 U}{\partial x^2}, & (x, t) \in [0, L] \times [0, T] \\ U(0, t) = U(L, t) = 0, & t \in [0, T] \\ U(x, 0) = \sin\left(\frac{2\pi x}{L}\right), & x \in [0, T] \end{cases} \quad (4.1)$$

where $\gamma = 0.005m^2/s$ and $L = 100m$. We adopt the leapfrog/DuFort-Frankel scheme (the central finite difference scheme in both the temporal and spatial directions) to numerically solve the viscous Burgers equation above (4.1), with $\Delta x = 1m$ as the spatial grid size ($d = 101$) and $\Delta t = 1s$ as the time step. The objective function $J(u_0)$ used for optimization (2.2) can be rewritten in the form of the norm square of perturbation as

$$J(u_0) = \|u(T)\|^2 = \sum_{i=1}^d u_i(T)^2.$$

Moreover, the constraint for the initial condition is set to be $\|u_0\| \leq \delta = 8 \times 10^{-4}m/s$. Under the setting $\epsilon = 10^{-8}$ for the definition of $\hat{J}(u_0)$ in (3.1), we carry out numerical experiments to calculate CNOP directly from the definition, by the adjoint-based method and the sample-based method with $n = 5$ and $n = 15$. The prediction time is set for two cases, $T = 30s$ and $T = 60s$, respectively. The CNOPs computed by the four algorithms are shown in Figure 1, and the actual running times are shown in Table 1.

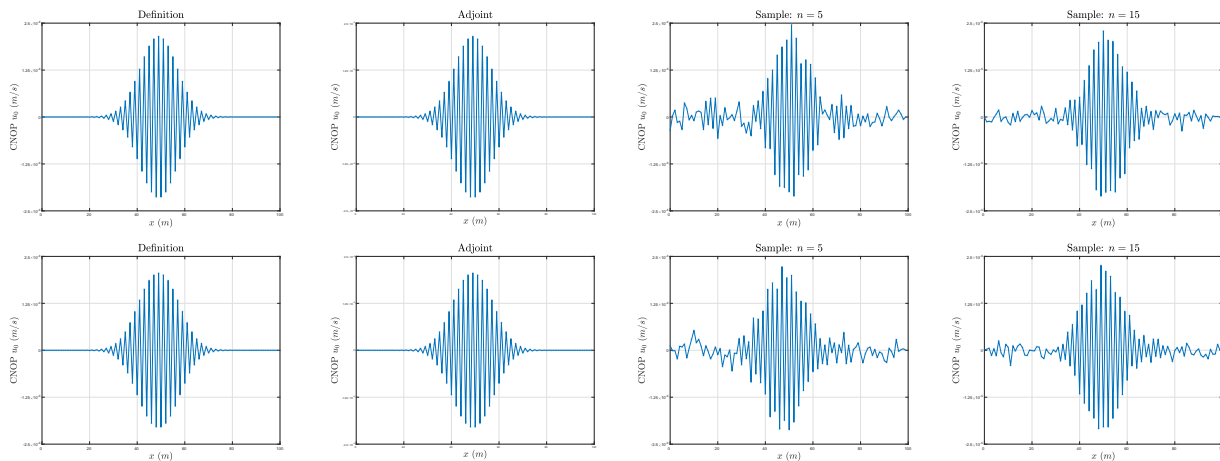


Figure 1: Spatial distributions of CNOP (m/s). Prediction time: on the top is $T = 30s$, and on the bottom is $T = 60s$. From left to right: Definition method, Adjoint method, Sample method ($n = 5$) and Sample method ($n = 15$).

From Figure 1, we can find that the CNOP obtained by the adjoint method is almost the same as that computed directly from the definition, taking the numerical gradient with the spatial grid set as $\alpha = 10^{-8}$, for both the two cases of prediction time $T = 30s$ and $T = 60s$. It is well-known that the actual running time for the adjoint method is far less than that directly computed from the definition, which is tested for the Burgers equation with small viscosity in Table 1. For the sample-based method, some fluctuating errors of the CNOP are shown in the spatial distributions (the right two columns of Figure 1) due to noise. However, the basic spatial pattern of CNOP can be obtained, even for the case with fewer samples $n = 5$. Furthermore, we can also find the actual running time to get the CNOP by taking the samples $n = 15$ is more or less in agreement with the adjoint method. Moreover, the actual running time in the sampling way decreases when we reduce the number of samples from $n = 15$ to $n = 5$.

The nonlinear time evolutions of all CNOPs in terms of norm squares $\|u(t)\|^2$, which are obtained by the four algorithms above, are in such good agreement as to appear to be identical in Figure 2 for

Time	Methods				
	Definition	Adjoint	Sample ($n = 5$)	Sample ($n = 15$)	
$T = 30s$	3.2788s	1.0066s	0.3836s	0.8889s	
$T = 60s$	6.3106s	1.4932s	0.6464s	1.4845s	

Table 1: Comparison of actual running time within the four algorithms for the prediction time, $T = 30s$ and $T = 60s$.

both the two cases of prediction time $T = 30s$ and $T = 60s$ respectively. For the case of prediction time $T = 30s$, the nonlinear time evolution of the CNOP in terms of norm square $\|u(t)\|^2$ is tiny before the perturbations start to proliferate approximately at the time $t = 20s$, and then the growth enlarges sharply. Similarly, the nonlinear time evolution tendency is almost the same as for the prediction time $T = 60s$ with the rapid growth time of the perturbations about $t = 50s$. Actually, from the top two figures of Figure 3, we can find that the most significant difference in the nonlinear time evolution of norm square of perturbations $\Delta\|u(t)\|^2$ is between the definition method and the sample-based method with $n = 5$ samples, which is less than $6 \times 10^{-7}m^2/s^2$ for the prediction time $T = 30s$ and $0.12m^2/s^2$ for the prediction time $T = 60s$ respectively. From the bottom two figures of Figure 3, this phenomenon can be observed further that the relative difference within the nonlinear time evolution $\Delta\|u(t)\|^2/\|u(t)\|^2$ is almost consistent with zero, except for a large ratio at the time $t = 11s$.

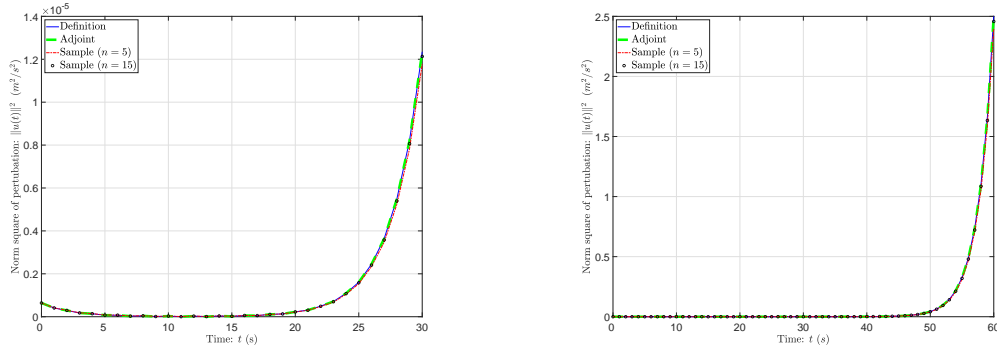


Figure 2: Nonlinear time evolutions of CNOP in terms of the norm square (m^2/s^2). Left: the prediction time is $T = 30s$; Right: the prediction time is $T = 60s$, respectively.

Based on all the demonstrations by the numerical experiments above, for both the figures (Figure 1 — Figure 3) and the table (Table 1), we utilize the sample-based method with the number $n = 5$ to obtain the CNOP within a relatively shorter time at the cost of losing accuracy, meanwhile get over the disadvantage of the massive storage space for the basic state and the running instability based on the linearization.

5 Summary and discussion

In this paper, we have introduced a sample-based algorithm to obtain the CNOPs, which rests on the high-dimensional Stokes' theorem and the law of large numbers. Meanwhile, we have also

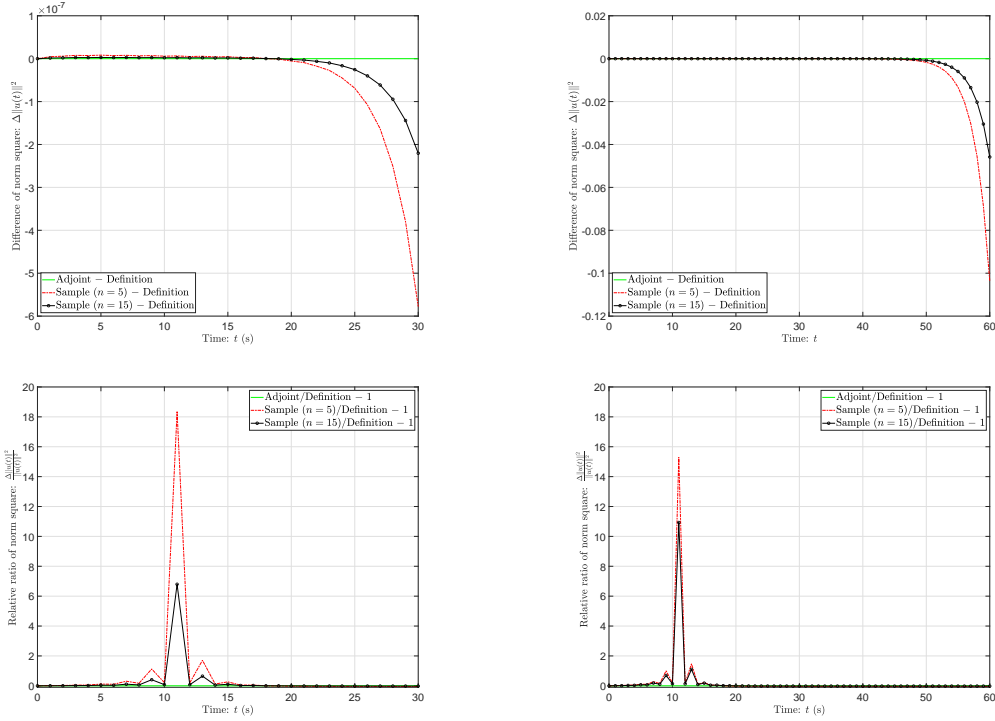


Figure 3: Nonlinear evolutions of CNOP in terms of the difference (m^2/s^2) and relative difference of norm square of perturbations. The top two figures are for the difference and the bottom two for the relative difference. Left: the prediction time is $T = 30s$; Right: the prediction time is $T = 60s$.

provided a rigorous concentration estimate for the exact gradient by the average of samples and compared the performance between the sample-based and the baseline algorithms by taking several numerical experiments. Compared with the classical adjoint-based method, this approach is easier to implement and saves a massive storage space of the basic state. When we reduce the number of samples to some extent, it reduces much more time to run the sample-based method, which can guarantee the CNOP obtained is almost consistent with some minor fluctuating errors oscillating in spatial distribution. Currently, the CNOP method has been widely applied to the predictability of atmospheric and oceanic motions. However, for an earth system model closer to nature, such as Community Earth System Model (CESM), there still exist many difficulties in obtaining the CNOP [Wang et al., 2020], or even for a high-resolution model, such as the Weather Research and Forecasting (WRF) Model, used widely in the operational forecasting [Yu et al., 2017]. Based on more and more reliable models developed in atmospheric science and oceanography, we remark on some extensions of the sample-based method to investigate them on the more complex models, theoretical or practical, to obtain the CNOPs. Firstly, to further test the validity of the sampling algorithm to calculate the CNOPs, we will start from an idealized ocean-atmosphere coupling model with its adjoint model, the Zebiak-Cane (ZC) model [Zebiak and Cane, 1987], which might characterize the oscillatory behavior of ENSO in amplitude and period based on oceanic wave dynamics. Mu et al. [2007] obtained the CNOP and studied the spring predictability barrier for El Niño events by applying the ZC model and its adjoint model. In addition, Mu et al. [2009] also employed the PSU/NCAR mesoscale model, known as the MM5 model, with its adjoint model

to explore the predictability of tropical cyclones by computing its CNOP. We will implement the sample-based methods to obtain the CNOPs on the above models and compare their performances with the adjoint-based methods. Secondly, based on the fact about the validity of the sampling algorithm, the CNOPs will be investigated for an earth system model or Atmosphere-Ocean General Circulation Models (AOGCMs) without its adjoint model. Meanwhile, we will take the sample-based algorithms to investigate further the nonlinear instability and predictability in a popular atmospheric blocking model, the nonlinear multiscale interaction model (NMI) [Luo et al., 2014], which also successfully exhibits an eddy-blocking matching mechanism.

Acknowledgments

We are indebted to Mu Mu for seriously reading the earlier version of this paper and giving his suggestions about this theoretical study. Bin Shi is also obligated to Ya-xiang Yuan, Ping Zhang, and Yu-hong Dai for their encouragement to understand and analyze the nonlinear phenomena in nature from the view of optimization at the early stage of this project.

References

- A. Barclay, P. E. Gill, and J. Ben Rosen. SQP methods and their application to numerical optimal control. In *Variational calculus, optimal control and applications*, pages 207–222. Springer, 1998.
- E. G. Birgin, J. M. Martínez, and M. Raydan. Nonmonotone spectral projected gradient methods on convex sets. *SIAM Journal on Optimization*, 10(4):1196–1211, 2000.
- L. Bottou, F. E. Curtis, and J. Nocedal. Optimization methods for large-scale machine learning. *SIAM Review*, 60(2):223–311, 2018.
- R. Buizza and T. N. Palmer. The singular-vector structure of the atmospheric global circulation. *J. Atmos. Sci.*, 52(9):1434–1456, 1995.
- L. Chen, W. Duan, and H. Xu. A SVD-based ensemble projection algorithm for calculating the conditional nonlinear optimal perturbation. *Science China Earth Sciences*, 58(3):385–394, 2015.
- W. Duan and J. Hu. The initial errors that induce a significant “spring predictability barrier” for El Niño events and their implications for target observation: Results from an earth system model. *Climate Dynamics*, 46(11):3599–3615, 2016.
- W. Duan, X. Liu, K. Zhu, and M. Mu. Exploring the initial errors that cause a significant “spring predictability barrier” for El Niño events. *Journal of Geophysical Research: Oceans*, 114(C4), 2009.
- E. T. Eady. Long waves and cyclone waves. *Tellus*, 1(3):33–52, 1949.
- B. F. Farrell. The initial growth of disturbances in a baroclinic flow. *J. Atmos. Sci.*, 39(8):1663–1686, 1982.
- B. F. Farrell and P. J. Ioannou. Generalized stability theory. Part I: Autonomous operators. *Journal of Atmospheric Sciences*, 53(14):2025–2040, 1996a.
- B. F. Farrell and P. J. Ioannou. Generalized stability theory. Part II: Nonautonomous operators. *Journal of Atmospheric Sciences*, 53(14):2041–2053, 1996b.
- Y. Fujii, H. Tsujino, N. Usui, H. Nakano, and M. Kamachi. Application of singular vector analysis to the Kuroshio large meander. *Journal of Geophysical Research: Oceans*, 113(C7), 2008.

- E. Kalnay. *Atmospheric modeling, data assimilation and predictability*. Cambridge university press, 2003.
- R. R. Kerswell. Nonlinear nonmodal stability theory. *Annual Review of Fluid Mechanics*, 50:319–345, 2018.
- C.-C. Lin. *The theory of hydrodynamic stability*. Cambridge University Press, Cambridge, UK., 1955.
- D. C. Liu and J. Nocedal. On the limited memory BFGS method for large scale optimization. *Mathematical programming*, 45(1):503–528, 1989.
- E. N. Lorenz. A study of the predictability of a 28-variable atmospheric model. *Tellus*, 17(3):321–333, 1965.
- D. Luo, J. Cha, L. Zhong, and A. Dai. A nonlinear multiscale interaction model for atmospheric blocking: The eddy-blocking matching mechanism. *Quarterly Journal of the Royal Meteorological Society*, 140(683):1785–1808, 2014.
- M. Mu. Nonlinear singular vectors and nonlinear singular values. *Science in China Series D: Earth Sciences*, 43(4):375–385, 2000.
- M. Mu and J. Wang. Nonlinear fastest growing perturbation and the first kind of predictability. *Science in China Series D: Earth Sciences*, 44(12):1128–1139, 2001.
- M. Mu and Q. Wang. Applications of nonlinear optimization approach to atmospheric and oceanic sciences. *SCIENTIA SINICA Mathematica*, 47(10):1207–1222, 2017.
- M. Mu, W. S. Duan, and B. Wang. Conditional nonlinear optimal perturbation and its applications. *Nonlinear Processes in Geophysics*, 10(6):493–501, 2003.
- M. Mu, L. Sun, and H. A. Dijkstra. The sensitivity and stability of the ocean’s thermohaline circulation to finite-amplitude perturbations. *Journal of Physical Oceanography*, 34(10):2305–2315, 2004.
- M. Mu, H. Xu, and W. Duan. A kind of initial errors related to “spring predictability barrier” for El Niño events in Zebiak-Cane model. *Geophysical Research Letters*, 34(3), 2007.
- M. Mu, F. Zhou, and H. Wang. A method for identifying the sensitive areas in targeted observations for tropical cyclone prediction: Conditional nonlinear optimal perturbation. *Monthly Weather Review*, 137(5):1623–1639, 2009.
- Navrose, H. G. Johnson, V. Brion, L. Jacquin, and J.-C. Robinet. Optimal perturbation for two-dimensional vortex systems: route to non-axisymmetric state. *Journal of Fluid Mechanics*, 855:922–952, 2018.
- A. S. Nemirovski and D. B. Yudin. Problem complexity and method efficiency in optimization. 1983.
- C. C. T. Pringle and R. R. Kerswell. Using nonlinear transient growth to construct the minimal seed for shear flow turbulence. *Physical review letters*, 105(15):154502, 2010.
- X. Qin and M. Mu. Influence of conditional nonlinear optimal perturbations sensitivity on typhoon track forecasts. *Quarterly Journal of the Royal Meteorological Society*, 138(662):185–197, 2012.
- L. Rayleigh. On the stability, or instability, of certain fluid motions. *Proceedings of the London Mathematical Society*, 1(1):57–72, 1879.
- R. M. Samelson and E. Tziperman. Instability of the chaotic ENSO: The growth-phase predictability barrier. *J. Atmos. Sci.*, 58(23):3613–3625, 2001.
- G. Sun and M. Mu. A new approach to identify the sensitivity and importance of physical parameters combination within numerical models using the Lund–Potsdam–Jena (LPJ) model as an example. *Theoretical and Applied Climatology*, 128(3):587–601, 2017.

- C. J. Thompson. Initial conditions for optimal growth in a coupled ocean–atmosphere model of ENSO. *J. Atmos. Sci.*, 55(4):537–557, 1998.
- R. Vershynin. *High-dimensional probability: An introduction with applications in data science*, volume 47. Cambridge university press, 2018.
- B. Wang and X. Tan. Conditional nonlinear optimal perturbations: Adjoint-free calculation method and preliminary test. *Monthly Weather Review*, 138(4):1043–1049, 2010.
- Q. Wang and M. Mu. A new application of conditional nonlinear optimal perturbation approach to boundary condition uncertainty. *Journal of Geophysical Research: Oceans*, 120(12):7979–7996, 2015.
- Q. Wang, M. Mu, and G. Sun. A useful approach to sensitivity and predictability studies in geophysical fluid dynamics: conditional non-linear optimal perturbation. *National Science Review*, 7(1):214–223, 2020.
- Y. Xue, M. A. Cane, and S. E. Zebiak. Predictability of a coupled model of ENSO using singular vector analysis. Part I: Optimal growth in seasonal background and ENSO cycles. *Mon. Wea. Rev.*, 125(9):2043–2056, 1997a.
- Y. Xue, M. A. Cane, S. E. Zebiak, and T. N. Palmer. Predictability of a coupled model of ENSO using singular vector analysis. Part II: Optimal growth and forecast skill. *Mon. Wea. Rev.*, 125(9):2057–2073, 1997b.
- H. Yu, H. Wang, Z. Meng, M. Mu, X.-Y. Huang, and X. Zhang. A WRF-based tool for forecast sensitivity to the initial perturbation: The conditional nonlinear optimal perturbations versus the first singular vector method and comparison to MM5. *Journal of Atmospheric and Oceanic Technology*, 34(1):187–206, 2017.
- S. Yuan, L. Zhao, and B. Mu. Parallel cooperative co-evolution based particle swarm optimization algorithm for solving conditional nonlinear optimal perturbation. In *International Conference on Neural Information Processing*, pages 87–95. Springer, 2015.
- L. Zanna, P. Heimbach, A. M. Moore, and E. Tziperman. Optimal excitation of interannual atlantic meridional overturning circulation variability. *Journal of Climate*, 24(2):413–427, 2011.
- S. E. Zebiak and M. A. Cane. A model El Niño–Southern Oscillation. *Monthly Weather Review*, 115(10):2262–2278, 1987.
- Q. Zheng, Z. Yang, J. Sha, and J. Yan. Conditional nonlinear optimal perturbations based on the particle swarm optimization and their applications to the predictability problems. *Nonlinear Processes in Geophysics*, 24(1):101–112, 2017.
- Z. Zu, M. Mu, and H. A. Dijkstra. Optimal initial excitations of decadal modification of the atlantic meridional overturning circulation under the prescribed heat and freshwater flux boundary conditions. *Journal of Physical Oceanography*, 46(7):2029–2047, 2016.

A Proof of Theorem 1

Lemma A.1. If $\hat{J}(u_0)$ is defined in (3.1), then the equation (3.2) is satisfied. Furthermore, under the same assumption of Theorem 1, the estimates for the objective value and gradient difference can be obtained as

$$\|\hat{J}(u_0) - J(u_0)\| \leq \frac{L\epsilon^2}{2}, \quad (\text{A.1})$$

$$\|\nabla \hat{J}(u_0) - \nabla J(u_0)\| \leq \frac{Ld\epsilon}{2}. \quad (\text{A.2})$$

Proof of Lemma A.1. Firstly, with the definition of $\hat{J}(u_0)$, we show the proof about the computation of gradient $\nabla \hat{J}(u_0)$ in (3.2).

- For $d = 1$, the gradient $\hat{J}(u_0)$ about u_0 can be computed as

$$\frac{d\hat{J}(u_0)}{du_0} = \frac{d}{du_0} \left(\frac{1}{2} \int_{-1}^1 J(u_0 + \epsilon v_0) dv_0 \right) = \frac{1}{2} \int_{-1}^1 \frac{dJ(u_0 + \epsilon v_0)}{\epsilon dv_0} dv_0 = \frac{J(u_0 + \epsilon) - J(u_0 - \epsilon)}{2\epsilon}.$$

- For the case of $d \geq 2$, we assume first $\mathbf{a} \in \mathbb{R}^d$ is an arbitrary vector. Then, the gradient $\nabla \hat{J}(u_0)$ satisfies the following equality as

$$\begin{aligned} \mathbf{a} \cdot \nabla \hat{J}(u_0) &= \int_{v_0 \in \mathbb{B}^d} \mathbf{a} \cdot \nabla_{u_0} J(u_0 + \epsilon v_0) dV \\ &= \frac{1}{\epsilon} \int_{v_0 \in \mathbb{B}^d} \nabla_{v_0} \cdot (J(u_0 + \epsilon v_0) \mathbf{a}) dV \\ &= \frac{1}{\epsilon} \int_{v_0 \in \mathbb{S}^{d-1}} J(u_0, k + \epsilon v_0) \mathbf{a} \cdot v_0 dS \\ &= \mathbf{a} \cdot \frac{1}{\epsilon} \int_{v_0 \in \mathbb{S}^{d-1}} J(u_0 + \epsilon v_0) v_0 dS. \end{aligned}$$

Since the vector \mathbf{a} is arbitrary, we can obtain the following equality as

$$\nabla \int_{v_0 \in \mathbb{B}^d} J(u_0 + \epsilon v_0) dV = \frac{1}{\epsilon} \int_{v_0 \in \mathbb{S}^{d-1}} J(u_0 + \epsilon v_0) v_0 dS.$$

Then, with d being the ratio of the surface area and the volume of \mathbb{B}^d , the representation of gradient in (3.2) is satisfied.

If J is continuously differentiable and satisfies the gradient Lipschitz condition, we can obtain the following inequality for J as

$$|J(u_0 + \epsilon v_0) - J(u_0) - \epsilon \langle \nabla J(u_0), v_0 \rangle| \leq \frac{L\epsilon^2}{2} \|v_0\|^2.$$

Since $\int_{v_0 \in \mathbb{B}^d} \langle \nabla J(u_0), v_0 \rangle dV = 0$, the estimate (A.1) can be obtained directly. For any $i \neq j \in \{1, \dots, d\}$, $v_{0,i}$ and $v_{0,j}$ are uncorrelated, that is,

$$\int_{v_0 \in \mathbb{S}^{d-1}} v_{0,i} v_{0,j} dS = 0;$$

for the case $i = j \in \{1, \dots, d\}$, we have

$$\int_{v_0 \in \mathbb{S}^{d-1}} v_{0,i}^2 dS = \frac{1}{d} \int_{v_0 \in \mathbb{S}^{d-1}} \left(\sum_{i=1}^d v_{0,i}^2 \right) dS = \frac{1}{d} \int_{v_0 \in \mathbb{S}^{d-1}} dS.$$

Then, with the row vector representation of v_0 , we can obtain the following equality as

$$\mathbb{E}_{v_0 \in \mathbb{S}^{d-1}} [v_0^T v_0] = \frac{1}{d} \cdot \mathbf{I}.$$

Furthermore, we can obtain the equivalent representation of the gradient $\nabla J(u_0)$ as

$$\nabla J(u_0) = \frac{d}{\epsilon} \cdot \mathbb{E}_{v_0 \in \mathbb{S}^{d-1}} [\epsilon \langle \nabla J(u_0), v_0 \rangle v_0].$$

Finally, with $\mathbb{E}_{v_0 \in \mathbb{S}^{d-1}}[v_0] = 0$, the norm of gradient difference is estimated as

$$\begin{aligned} \|\nabla \hat{J}(u_0) - \nabla J(u_0)\| &\leq \left\| \frac{d}{\epsilon} \cdot \mathbb{E}_{v_0 \in \mathbb{S}^{d-1}} [(J(u_0 + \epsilon v_0) - J(u_0)) v_0] - \frac{d}{\epsilon} \cdot \mathbb{E}_{v_0 \in \mathbb{S}^{d-1}} [\epsilon \langle \nabla J(u_0), v_0 \rangle v_0] \right\| \\ &\leq \frac{d}{\epsilon} \cdot \mathbb{E}_{v_0 \in \mathbb{S}^{d-1}} [\|J(u_0 + \epsilon v_0) - J(u_0) - \epsilon \langle \nabla J(u_0), v_0 \rangle\| \cdot \|v_0\|] \\ &\leq \frac{Ld\epsilon}{2}, \end{aligned}$$

where the last inequality follows the gradient Lipschitz condition. \square

Considering any $\epsilon > 0$, in order to proceed with the concentration inequality, we still need to know the random variable $J(u_0 + \epsilon v_0)$ for $v_0 \sim \text{Unif}(\mathbb{S}^{d-1})$ is sub-gaussian. Hence, we first introduce the following lemma.

Lemma A.2 (Proposition 2.5.2 in [Vershynin \[2018\]](#)). Let X be a random variable. If there exist two constants $K_1, K_2 > 0$ such that the moment generating function of X^2 is bounded, that is,

$$\mathbb{E} \left[\exp \left(\frac{X^2}{K_1^2} \right) \right] \leq K_2,$$

then the random variable X is sub-gaussian.

Since $J(u_0 + \epsilon v_0)$ is bounded on \mathbb{S}^{d-1} , $\exp((J(u_0 + \epsilon v_0))^2/K_1^2)$ is integrable on \mathbb{S}^{d-1} for any $K_1 > 0$, that is, there exists a constant $K_2 > 0$ such that

$$\mathbb{E}_{v_0 \in \mathbb{S}^{d-1}} \left[\exp \left(\frac{J(u_0 + \epsilon v_0)^2}{K_1^2} \right) \right] \leq K_2.$$

The random variable $J(u_0 + \epsilon v_0)$ is sub-gaussian. Therefore, for any fixed vector $v'_0 \in \mathbb{S}^{d-1}$, we know the random variable $J(u_0 + \epsilon v_0) \langle v_0, v'_0 \rangle$ is sub-gaussian. Now, we introduce the following lemma to proceed with the concentration inequality.

Lemma A.3 (Theorem 2.6.3 in [Vershynin \[2018\]](#)). Let X_1, \dots, X_n be independent, mean zero, sub-gaussian random variables, and $a = (a_1, \dots, a_n) \in \mathbb{R}^n$. Then, for every $t \geq 0$, we have

$$\Pr \left(\left| \sum_{i=1}^n a_i X_i \right| \geq t \right) \leq 2 \exp \left(-\frac{ct^2}{K^2 \|a\|^2} \right),$$

where $K = \max_{1 \leq i \leq n} \|X_i\|_{\psi_2}$.²

²The subgaussian norm of a random variable X is defined as

$$\|X\|_{\psi_2} = \inf \left\{ t > 0 : \mathbb{E} \exp \left(\frac{X^2}{t^2} \right) \leq 2 \right\}.$$

With Lemma A.1 and Lemma A.3, we can obtain the concentration inequality for samples as

$$\Pr \left(\left| \frac{d}{n\epsilon} \sum_{i=1}^n \langle J(u_0 + \epsilon v_{0,i}) v_{0,i} v'_0 \rangle - \langle \nabla \hat{J}(u_0), v'_0 \rangle \right| \geq t \right) \leq 2 \exp \left(-\frac{cnt^2}{K^2} \right).$$

Since v'_0 is a unit vector on \mathbb{S}^{d-1} , by the Cauchy-Schwarz inequality, we can proceed with the concentration estimate as

$$\Pr \left(\left\| \frac{d}{n\epsilon} \sum_{i=1}^n J(u_0 + \epsilon v_{0,i}) v_{0,i} - \nabla \hat{J}(u_0) \right\| \geq t \right) \leq 2 \exp \left(-\frac{cnt^2}{K^2} \right).$$

By the triangle inequality, the concentration inequality can proceed with the estimate of gradient difference (A.2) as

$$\Pr \left(\left\| \frac{d}{n\epsilon} \sum_{i=1}^n J(u_0 + \epsilon v_{0,i}) v_{0,i} - \nabla J(u_0) \right\| \geq t - \frac{Ld\epsilon}{2} \right) \leq 2 \exp \left(-\frac{cnt^2}{K^2} \right)$$

for any $t > Ld\epsilon/2$. Taking $C = c/K^2$, the proof of Theorem 1 is complete.